Theoretical Studies on the Insertions of Unsymmetrical Alkynes into the Metal−Carbon Bond of Phosphanickelacycles: Electronic Factors

Stuart A. Macgregor*,† and Eric Wenger‡

Department of Chemistry, Heriot-Watt University, Riccarton, Edinburgh EH14 4AS, U.K., and Research School of Chemistry, Australian National University, Canberra, Australian Central Territory 0200, Australia

Received September 4, 2001

Density functional calculations have been employed to study the insertion reactions of alkynes (RC≡CR′: R = H, R′ = H, Me, CF_3, Ph; R = Me, R′ = Ph; R = CO_2H, R′ = H, Me, CF_3, Ph) with the model phosphanickelacycle [NiBr(CH=CHCH$_2$PH$_2$-$\kappa C,P$)(PH_3)]. Calculations with HC≡CH indicate that associative processes with insertion via 5-coordinate intermediates are preferred kinetically over an alternative mechanism involving initial displacement of a PH_3 ligand. Two possible trigonal-bipyramidal 5-coordinate intermediates were located with either Br or PH_3 occupying an axial position trans to the Ni−vinyl bond. The preference for an associative process was confirmed with HO_2CC≡CH and HC≡CMe. Computed 5-coordinate transition state energies for unsymmetrical alkynes are generally consistent with the regioselectivities observed with experimental analogues. One exception is HC≡CCF_3, for which the wrong regioisomer is marginally favored, although the computed energy difference between the transition states leading to opposite regioisomers is negligible. Both the observed and calculated results are discussed in terms of a simple model for predicting the insertion regioselectivities based on the polarization of the alkyne $\pi_\perp$ orbital. In all cases, this model accounts well for the experimental regioselectivities but analysis of the computational results shows the success of this approach depends on both the alkyne and the 5-coordinate intermediate from which the insertion occurs. In particular, when electron-withdrawing substituents are present, a swap in regioselectivity is often predicted, depending upon whether insertion proceeds from the isomer with Br axial or from that with PH_3 axial.

1. Introduction

The insertion of an unsaturated molecule into a metal−carbon bond is a fundamental reaction in organometallic chemistry, which has been exploited in both organic syntheses and industrial processes.[1] Detailed experimental studies have been carried out on alkene and CO insertions,[2,3] and these have been underpinned by extensive theoretical investigations.[4] Alkyne insertion reactions have also received considerable attention, especially in the context of transition-metal-catalyzed cyclotrimerization and oligomerization reactions.[5,6] More recently, the insertion of an alkyne into the metal−carbon σ-bond of a metallacycle has become a synthetically useful process, because cyclometalated compounds can often be prepared directly by cleavage of a C−H bond close to a suitable donor atom.[7] In particular, alkyne reactions with palladacycles[8] or nickelacycles[9] have found wide application in the synthesis of important polycyclic and heterocyclic molecules. While the reactions of the nickel complexes remain mainly stoichiometric, many powerful catalytic processes have been developed with palladium.[8g]

The use of unsymmetrical alkynes in such reactions, however, results in important regiochemical consider-

† Heriot-Watt University. Fax: +44 (131) 451 3180. E-mail: s.a.macgregor@hw.ac.uk.

‡ Australian National University. Fax: +61 (2) 6125 0750. E-mail: wenger@rsc.anu.edu.au.

(1) Collman, J. P.; Hegedus, L. S.; Norton, J. R.; Finke, R. G. *Principles and Applications of Organotransition Metal Chemistry*; University Science Books: Mill Valley, CA, 1987.

(2) Boffa, L. S.; Novak, B. M. *Chem. Rev.* **2000**, *100*, 1479.

(3) Ittel, S. D.; Johnson, L. K.; Brookhart, M. *Chem. Rev.* **2000**, *100*, 1169.

(4) Torrent, M.; Solà, M.; Frenking, G. *Chem. Rev.* **2000**, *100*, 439.

(5) For pioneering work in the field, see: (a) Maitlis, P. M. *Pure Appl. Chem.* **1972**, *30*, 427. (b) Maitlis, P. M. *Pure Appl. Chem.* **1973**, *33*, 489. (c) Maitlis, P. M. *Acc. Chem. Res.* **1976**, *9*, 93. (d) Maitlis, P. M. *J. Organomet. Chem.* **1980**, *200*, 161.

(6) Selected reviews: (a) Vollhardt, K. P. C. *Acc. Chem. Res.* **1977**, *10*, 1. (b) Jolly, P. W. In *Comprehensive Organometallic Chemistry*; Wilkinson, G., Stone, F. G. A., Abel, E. W., Eds.; Pergamon: Oxford, U.K., 1982; Vol. 8, p 649. (c) Winter, M. J. In *The Chemistry of the Metal−Carbon Bond*; Hartley, F. R., Patai, S., Eds.; Wiley: New York, 1985; Vol. 3, pp 259−294. (d) Schore, N. E. In *Comprehensive Organic Synthesis*; Trost, B. M., Fleming, I., Paquette, L. A., Eds.; Pergamon: Oxford, U.K., 1991; Vol. 5, pp 1129−1162. (e) Saito, S.; Yamamoto, Y. *Chem. Rev.* **2000**, *100*, 2901.

(7) (a) Bruce, M. I. *Angew. Chem., Int. Ed. Engl.* **1977**, *16*, 73. (b) Omae, I. *Organometallic Intramolecular Coordination Compounds*; Elsevier: Amsterdam, 1986. (c) Ryabov, A. D. *Chem. Rev.* **1990**, *90*, 403.

(8) (a) Ryabov, A. D. *Synthesis* **1985**, 233. (b) Lindner, E. *Adv. Heterocycl. Chem.* **1986**, *39*, 237. (c) Pfeffer, M. *Recl. Trav. Chim. Pays-Bas* **1990**, *109*, 567. (d) Heck, R. F.; Wu, G.; Tao, W.; Rheingold, A. L. In *Catalysis of Organic Reactions*; Blackburn, D. W., Ed.; Dekker: New York, 1990. (e) Spencer, J.; Pfeffer, M. In *Advances in Metal-Organic Chemistry*; Liebeskind, L. S., Ed.; JAI Press: Stamford, CT, 1998; Vol. 6, p 104. (f) Cacchi, S. *J. Organomet. Chem.* **1999**, *576*, 42. (g) Larock, R. C. *J. Organomet. Chem.* **1999**, *576*, 111.

10.1021/om010795y CCC: $22.00 © 2002 American Chemical Society
Publication on Web 02/20/2002

Scheme 1

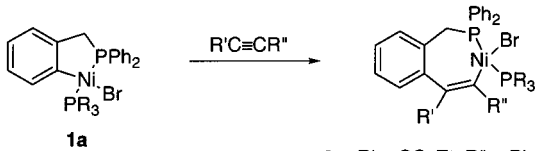

1a
1b

a: $PR_3 = PEt_3$
b: $PR_3 = PPhBz_2$

2a: R' = CO_2Et, R" = Ph

3a: R' = CO_2Me, R" = Me

3b: R' = CO_2Me, R" = Me (major)
4b: R' = Me, R" = CO_2Me

5a: R' = H, R" = CO_2Me
6a: R' = CO_2Me, R" = H (trace)

5b: R' = H, R" = CO_2Me (major)
6b: R' = CO_2Me, R" = H

7a: R' = H, R" = $CO_2{}^tBu$ (major)
8a: R' = $CO_2{}^tBu$, R" = H

9b: R' = CF_3, R" = CO_2Et

10a: R' = H, R" = ^tBu

11a: R' = H, R" = Ph

11b: R' = H, R" = Ph

12b: R' = Et, R" = Ph (major)
13b: R' = Ph, R" = Et

14b: R' = H, R" = CF_3 [a]
15b: R' = CF_3, R" = H (major)

[a] Unpublished results; see ref 30.

ations. Several mechanistic studies of the insertions of alkynes into Ni−C and Pd−C bonds have been reported,[10] but the factors governing the regiochemistry of these reactions remain unclear. For example, two investigations of the insertions of ^{t}BuC≡CMe into Ni−C[10c] and Pd−C[11] bonds have concluded that these reactions were under steric control, and this argument has been generally accepted for the insertions of alkynes into Pd−aryl bonds.[8e,f,12] However, the regioselectivities of the reactions of ester-activated alkynes with nickelaindenes[13] or alkynes in general with phosphanickelacycles[14] are better accounted for by invoking electronic factors. In the latter study,[14] a wide range of alkynes have been reacted with the complexes [NiBr($C_6H_4CH_2$-PPh_2-$\kappa C,P$)(L)] (L = PEt_3 (**1a**), PBz_2Ph (**1b**); Bz = benzyl, CH_2Ph) (Scheme 1) to form seven-membered metallacycles (**2**−**15**) by insertion into the Ni−C bond. Several alkyne/nickelacycle combinations produced effectively complete regioselectivities (e.g. **2a**, **3a**, **9b**, **10a**, and **11a**,**b**). However, in some cases, weaker regioselectivities were observed and isomeric ratios were sensitive to increased steric bulk either in the nickel coordination sphere (**3a** vs **3b/4b**; **5a/6a** vs **5b/6b**) or at the alkyne itself (**5a/6a** vs **7a/8a**).

To investigate the role that electronic factors may play in controlling the alkyne insertion process, a preliminary DFT study of a series of model alkynes was performed.[14] The results suggested a correlation between the electronic distribution of the $\pi_\perp$ HOMO of the alkyne and the regioselectivity of insertion. In all cases the polarization of the $\pi_\perp$ orbitals was found to be related to the major regioisomer produced and, in particular, the highly polarized $\pi_\perp$ orbitals computed for RC≡CPh (R = H, CO_2H) and HC≡CMe were consistent with the clean regioselectivities observed with experimental analogues. In addition, the reversal of regioselectivity seen when comparing MeC≡CCO_2Me (where products with the ester group in the β-position predominate) and CF_3C≡CCO_2Et (where CO_2Et is observed in the α-position) was also successfully rationalized by a change in polarization of the alkyne $\pi_\perp$ HOMO. Our interpretation of these results was that a preferential interaction of the alkyne $\pi_\perp$ HOMO with the Ni−C bond occurs, in which the alkyne carbon bearing the larger p-orbital coefficient is responsible for the C−C bond formation.

To date, relatively few theoretical studies of alkyne insertion reactions with group 10 metal complexes have been reported.[15] de Vaal and Dedieu investigated the insertion of acetylene into the Pd−CH_3 bond of the [Pd(CH_3)(NH_3)Cl(C_2H_2)] complex.[16] Using CAS-SCF//RHF and MRCI//RHF calculations, they found the Pd−acetylene interaction to be rather weak and located a planar insertion transition state with an activation energy of around 70 kJ/mol. The insertion process was exothermic by approximately 90 kJ/mol. The only theoretical study of the regioselectivity of alkyne insertion was performed by Nakatsuji and co-workers, who investigated the silastannation of unsymmetrical alkynes, RC≡CH (R = H, Me, CN, OMe), with $H_3Si-SnH_3$ catalyzed by the model complex [Pd(PH_3)$_2$].[17] Using RHF calculations, they again found planar insertion transition states were favored, with those leading to insertion into the Pd−Sn bond via migration of Sn to the terminal carbon being lowest in energy. These workers put forward two electronic factors which control the alkyne insertion process on the basis of frontier molecular orbital considerations. First, the overall reactivity of an alkyne (in terms of the computed activation energy) is governed by back-donation from the Pd−Sn bond to the in-plane π* LUMO of the alkyne. Alkynes with electron-withdrawing substituents (most stable LUMOs) are therefore more reactive (R = CN > OCH_3 > H > Me). Second, the regioselectivity is determined by forward donation from the alkyne in-plane π HOMO to the LUMO of the metal fragment,

(9) (a) Cámpora, J.; Paneque, M.; Poveda, M. L.; Carmona, E. *Synlett* **1994**, 465. (b) Smith, A. K. In *Comprehensive Organometallic Chemistry II*; Abel, E. W., Stone, F. G. A., Wilkinson, G., Puddephatt, R. J., Eds.; Elsevier: Oxford, U.K., 1995; Vol. 9, p 29. (c) Cámpora, J.; Palma, P.; Carmona, E. *Coord. Chem. Rev.* **1999**, *193*−*195*, 207. (d) Echavarren, A. M.; Castaño, A. M. In *Advances in Metal-Organic Chemistry*; Liebeskind, L. S., Ed.; JAI Press: Stamford, CT, 1998; Vol. 6, p 1. (e) Bennett, M. A.; Schwemlein, H. P. *Angew. Chem., Int. Ed. Engl.* **1989**, *28*, 1296. (f) Bennett, M. A.; Wenger, E. *Chem. Ber./Recl.* **1997**, *130*, 1029. (g) Jones, W. M.; Klosin, J. *Adv. Organomet. Chem.* **1998**, *42*, 147.

(10) (a) Martinez, M.; Muller, G.; Panyella, D.; Rocamora, M.; Solans, X.; Font-Bardía, M. *Organometallics* **1995**, *14*, 5552. (b) Samsel, E. G.; Norton, J. R. *J. Am. Chem. Soc.* **1984**, *106*, 5505. (c) Huggins, J. M.; Bergman, R. G. *J. Am. Chem. Soc.* **1981**, *103*, 3002−3011. (d) Ryabov, A. D.; van Eldik, R.; Le Borgne, G.; Pfeffer, M. *Organometallics* **1993**, *12*, 1386. (e) Ferstl, W.; Sakodinskaya, I. K.; Beydoun-Sutter, N.; Le Borgne, G.; Pfeffer, M.; Ryabov, A. D. *Organometallics* **1997**, *16*, 411.

(11) Spencer, J.; Pfeffer, M.; Kyritsakas, N.; Fischer, J. *Organometallics* **1995**, *14*, 2214.

(12) Abad, J.-A. *Gazz. Chim. Ital.* **1997**, *127*, 119.

(13) Bennett, M. A.; Wenger, E. *Organometallics* **1995**, *14*, 1267.

(14) Edwards, A. J.; Macgregor, S. A.; Rae, A. D.; Wenger, E.; Willis, A. C. *Organometallics* **2001**, *20*, 2864.

(15) (a) Dedieu, A. *Chem. Rev.* **2000**, *100*, 543. (b) Niu, S.; Hall, M. B. *Chem. Rev.* **2000**, *100*, 353.

(16) de Vaal, P.; Dedieu, A. *J. Organomet. Chem.* **1994**, *478*, 121.

(17) Hada, M.; Tanaka, Y.; Ito, M.; Murakami, M.; Amii, H.; Ito, Y.; Nakatsuji, H. *J. Am. Chem. Soc.* **1994**, *116*, 8754.

which is dominated by Sn p-orbital character. This idea is consistent with the polarization of the HOMOs of the substituted alkynes toward the terminal carbon. Electronic control of regioselectivity is therefore related to the energy of the alkyne HOMO and was less effective for R = CN (more stable HOMO) compared to R = Me, OMe. In this paper we aim to use density functional theory to see whether these ideas can be applied to the insertion reactions of unsymmetrical alkynes with [NiBr($C_6H_4CH_2PPh_2$-$\kappa C,P$)(L)] complexes, using the model complex [NiBr(CH=$CHCH_2PH_2$-$\kappa C,P$)(PH_3)] (**16**). Some of these results have been reported in a preliminary form in a recent perspective paper.[18]

2. Computational Details

All calculations used the Amsterdam Density Functional program ADF1999.[19] All geometry optimizations used a triple-ζ-STO basis set for Ni (ADF basis IV), while the other atoms were described by a double-ζ plus polarization STO basis set (ADF basis III). The frozen-core approximation was employed with the 1s electrons of C, O, and F atoms, up to and including the 2p electrons of P and Ni and the 3d electrons of Br. All geometry optimizations used the procedure developed by Versluis and Ziegler[20] and incorporated the gradient corrections of Becke[21] (exchange) and Perdew[22] (correlation) as well as the quasi-relativistic corrections of Snijders and co-workers.[23] The energies of all optimized structures were then recalculated using a triple-ζ-STO basis extended by two polarization functions for all nonmetal atoms (ADF basis V). For the model calculations with HC≡CH all stationary points were fully optimized and subsequently characterized using numerical frequency analyses[24] as being either minima (no imaginary frequencies) or transition states (one imaginary frequency). For the insertion reactions of HC≡CMe, HC≡CCO_2H, and MeC≡CCO_2H all stationary points were fully optimized, but full frequency analyses were not carried out due to the large size of the species involved; the computed geometries were analogous to those obtained with HC≡CH. We have also tested the functional dependency of our results by fully reoptimizing the lowest lying 5-coordinate transition states leading to both α- and β-regioselectivities for the insertions of HC≡CMe, HC≡CCO_2H, and MeC≡CCO_2H using the gradient corrections of Perdew and Wang.[25] In all cases energy differences changed by less than 0.5 kJ/mol. In a more general procedure, again due to the large size of several of the alkynes and the number of structures involved, transition state geometries and energies were not fully optimized but were instead estimated via constrained-geometry calculations in which the C^{β}−Ni−C^{γ} angle was frozen at the value computed in the analogous transition state structures located with HC≡CH (**17TSa/c** and **18TSa/c**, see main text). Experience with both alkyne and alkene migratory insertion reactions has shown that very similar transition state geometries are found for a series of related substrates or metal complexes and that the potential energy surface around the transition state is relatively flat. Nonetheless, this approach was tested with HC≡CMe, HC≡CCO_2H, and MeC≡CCO_2H, where the constrained-geometry results were compared with those derived from the full transition state searches. Only small differences in geometry between these two approaches were seen; for example, the maximum variation in the C^{β}−Ni−C^{γ} angle was 2.4°. In addition, differences in energy between constrained and full transition state optimizations were generally less than 1 kJ/mol. The only exception to this was for one transition state located with HC≡CMe, where a difference of 2.9 kJ/mol was computed. This could be traced to a different orientation of the Me group in the full optimization result. Therefore, for the constrained-geometry transition states the possibility of alternative low-energy conformations for the alkyne substituents was checked by computing energy profiles for rotation around each C_{alkyne}−R bond. If necessary, further geometry optimizations were then performed with the lowest energy results being reported.

3. Results

(a) Insertion Reaction of Acetylene with [NiBr(CH=$CHCH_2PH_2$-$\kappa C,P$)(PH_3)] (16). The computed structure of the model complex **16** is shown in Figure 1, where it is compared with that of the reported chloro analogue [NiCl(*o*-$C_6H_4CH_2PPh_2$-$\kappa C,P$)(PBz_3)].[26] The computed nickel−ligand bond lengths are generally shorter than those in the experimental structure, probably due to the use of PH_3 as a model ligand. This may also affect the trans ligand angles at Ni, where a significant distortion away from a square-planar structure is seen experimentally, presumably again as a response to steric encumbrance. The vinyl C=C double bond of the model metallacycle is also shorter than the equivalent aromatic C=C bond of the experimental system, as expected, but **16** can nevertheless be considered as a fair representation of the experimental species.

To establish the basic features of the alkyne insertion process with **16**, reaction profiles were computed for the simple case of acetylene. Both an associative mechanism with alkyne insertion from a 5-coordinate intermediate (pathway **A**, Scheme 2) and a mechanism involving initial PH_3 displacement with insertion via a 4-coordinate species (pathway **B**) were considered.

For the associative mechanism (**A**), a number of geometric isomers are in principle possible for the 5-coordinate intermediate formed upon binding of acetylene to **16**, and these were systematically assessed via a series of constrained-geometry calculations on trigonal-bipyramidal structures in which the angles at nickel between axial ligands and those between equatorial ligands were frozen at 180 and 120°, respectively. For each trigonal-bipyramidal form, two structures corresponding to two perpendicular orientations of the alkyne were considered. Upon further optimization with these constraints removed, all species collapsed to one of three minimum trigonal-bipyramidal structures. Two of these, **17** and **18**, are shown in Figure 1. Although we have not searched specifically for square-pyramidal structures, we expect our stepwise optimization procedure would have located such species if they existed as local minima.

(18) Bennett, M. A.; Macgregor, S. A.; Wenger, E. *Helv. Chim. Acta* **2001**, *84*, 3084.

(19) (a) Baerends, E. J.; Ellis, D. E.; Ros, P. *Chem. Phys.* **1973**, *2*, 41. (b) te Velde, G.; Baerends, E. J. *J. Comput. Phys.* **1992**, *99*, 84. (c) Fonseca Guerra, C.; Snijders, J. G.; te Velde, G.; Baerends, E. J. *Theor. Chem. Acta* **1998**, *99*, 391.

(20) (a) Versluis, L.; Ziegler, T. *Chem. Phys.* **1988**, *88*, 322. (b) Fan, L.; Ziegler, T. *J. Am. Chem. Soc.* **1992**, *114*, 10890.

(21) Becke, A. D. *Phys. Rev. A* **1988**, *38*, 3098.

(22) Perdew, J. P. *Phys. Rev. B* **1986**, *33*, 8822.

(23) (a) Snijders, J. G.; Baerends, E. J.; Ros, P. *Mol. Phys.* **1979**, *38*, 1909. (b) Ziegler, T.; Tschinke, V.; Baerends, E. J.; Snijders, J. G.; Ravenek, W. *J. Phys. Chem.* **1989**, *93*, 3050. (c) van Lenthe, E.; Baerends, E. J.; Snijders, J. G. *J. Chem. Phys.* **1993**, *99*, 4597.

(24) Fan, L.; Ziegler, T. *J. Chem. Phys.* **1992**, *96*, 9005. (b) Fan, L. Ziegler, T. *J. Chem. Phys.* **1992**, *96*, 6937.

(25) Perdew, J. P.; Chevary, J. A.; Vosko, S. H.; Jackson, K. A.; Pederson, M. R.; Singh, D. J.; Fiolhais, C. *Phys. Rev. B* **1992**, *46*, 6671.

(26) Muller, G.; Panyella, D.; Rocamora, M.; Sales, J.; Font-Bardía, M.; Solans, X. *J. Chem. Soc., Dalton Trans.* **1993**, 2959.

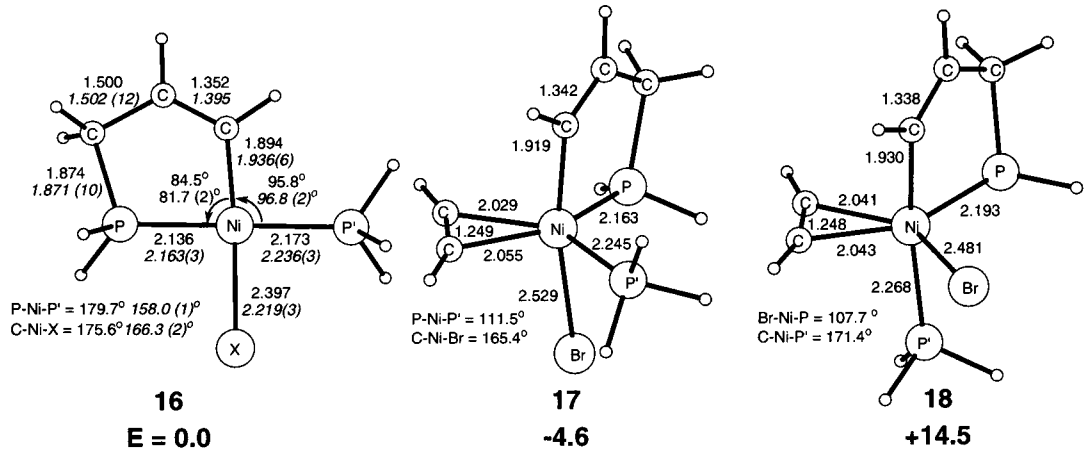

Figure 1. Optimized geometries (distances in Å and angles in deg) and relative energies (kJ/mol) for [NiX(CH═CHCH$_2$-PH$_2$-$\kappa C,P$)(PH$_3$)] (**16**; X = Br) and the 5-coordinate adducts **17** and **18**. The energy of **16** includes that of free acetylene and is set to zero. For **16**, experimental data for [NiX(*o*-C$_6$H$_4$CH$_2$PPh$_2$-$\kappa C,P$)(PBz$_3$)] (X = Cl), taken from ref 26, are given in italics for comparison.

Scheme 2

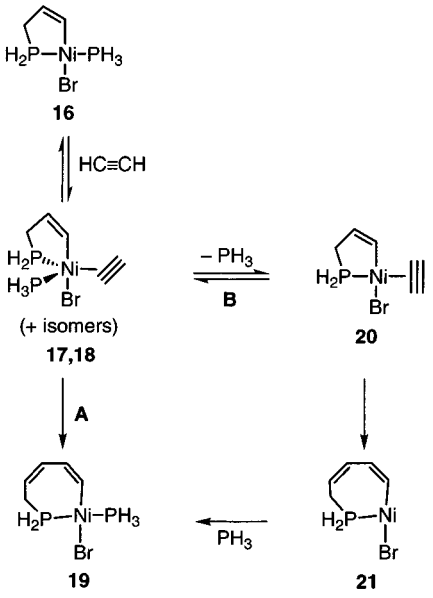

For both **17** and **18**, a P$_{eq}$−C$_{ax}$ binding mode for the chelate ligand is found; the alkyne ligand lies in the equatorial plane while either Br (**17**) or PH$_3$ (**18**) occupies the second axial site. Isomer **17** is −4.6 kJ/mol more stable, while **18** is 14.5 kJ/mol less stable, than the isolated reactants. A third isomer (E = +46.1 kJ/mol) was also located; however, its structure features an axial alkyne ligand trans to the vinyl arm of the metallacycle and is therefore not relevant for the insertion reaction.

For each 5-coordinate intermediate **17** and **18**, two insertion pathways are possible, depending on whether the alkyne rotates clockwise (**c**) or anticlockwise (**a**) with respect to the Ni−alkyne midpoint axis (Figure 2). In all the transition state geometries, the C$^\beta$−C$^\alpha$−Ni−C$^\gamma$ unit is distinctly nonplanar, with its torsion angle being around 40°. This arrangement is different from the transition states located by de Vaal and Dedieu[16] and Nakatsuji and co-workers[17] in their studies of alkyne insertions into Pd−R bonds. In those cases, the reactions took place from 4-coordinate species in which the acetylenic C≡C and Pd−R bonds were already coplanar. In **17** and **18**, the alkyne is perpendicular to the Ni−vinyl bond and so must rotate before insertion can occur. However, this process is still incomplete when the computed transition states are reached. It may be that a coplanar C$^\beta$−C$^\alpha$−Ni−C$^\gamma$ unit is avoided in these systems, as it would bring the hydrogens of both sp^2-hybridized C$^\beta$ and C$^\gamma$ atoms too close together. Another possibility is that the vinyl π system may be involved in C−C bond formation during the insertion process, which would avoid the requirement of a planar four-centered transition state (see below).[27] Relative to **17** and **18**, the corresponding insertion transition states (Figure 2) are also characterized by a lengthening of the Ni−C$^\gamma$ bond with a complementary shortening of the other Ni−L$_{ax}$ bond, a slight lengthening of the C$^\alpha$−C$^\beta$ and C$^\gamma$−C$^\delta$ bonds, and a marked lengthening of the Ni−L$_{eq}$ bond that was initially adjacent to C$^\alpha$ (viz., Ni−PH$_3$ for **c** rotation and Ni−PH$_2$ for **a** rotation). Three of the four transition states (**17TSc**, **17TSa**, and **18TSa**) are of similar energy (E = +52.4−56.4 kJ/mol), while the fourth (**18TSc**) is at slightly higher energy (+62.5 kJ/mol). Activation barriers, relative to the 5-coordinate species, are lower from **18**, possibly due to the higher trans influence of the PH$_3$ ligand, which weakens the Ni−C$^\gamma$ bond. However, overall there is no clear preference for insertion from one or the other of the 5-coordinate intermediates.[28]

Calculations on the 4-coordinate insertion product [NiBr(CH═CHCH═CHCH$_2$PH$_2$-$\kappa C,P$)(PH$_3$)] (**19**) reproduce the general features reported for the X-ray crystallographic structures of related species, in particular the boat-shaped configuration of the seven-membered metallacyclic ring (Figure 3). Comparison with the experimental structure of [NiBr{*o*-C(CO$_2$Me)═CHC$_6$H$_4$CH$_2$-PPh$_2$-$\kappa C,P$}(PPhBz$_2$)] (**5b**)[14] shows that the bond distances are reasonably well reproduced, while deviations in computed and experimental angles, most notably the Br−Ni−PH$_3$ angle, can again be attributed to the

(27) A similar transition state structure for an alkyne insertion reaction exploiting the alkyne $\pi_\perp$ orbitals has been suggested: Thorn, D. L.; Hoffmann, R. *J. Am. Chem. Soc.* **1978**, *100*, 2079.

(28) Implicit in this statement and throughout all this work is the assumption of kinetic control of reactivity, consistent with the low temperatures at which these insertion reactions occur experimentally. The favoured route therefore corresponds to that with the lowest energy pathway for insertion: viz., the lowest transition state energy.

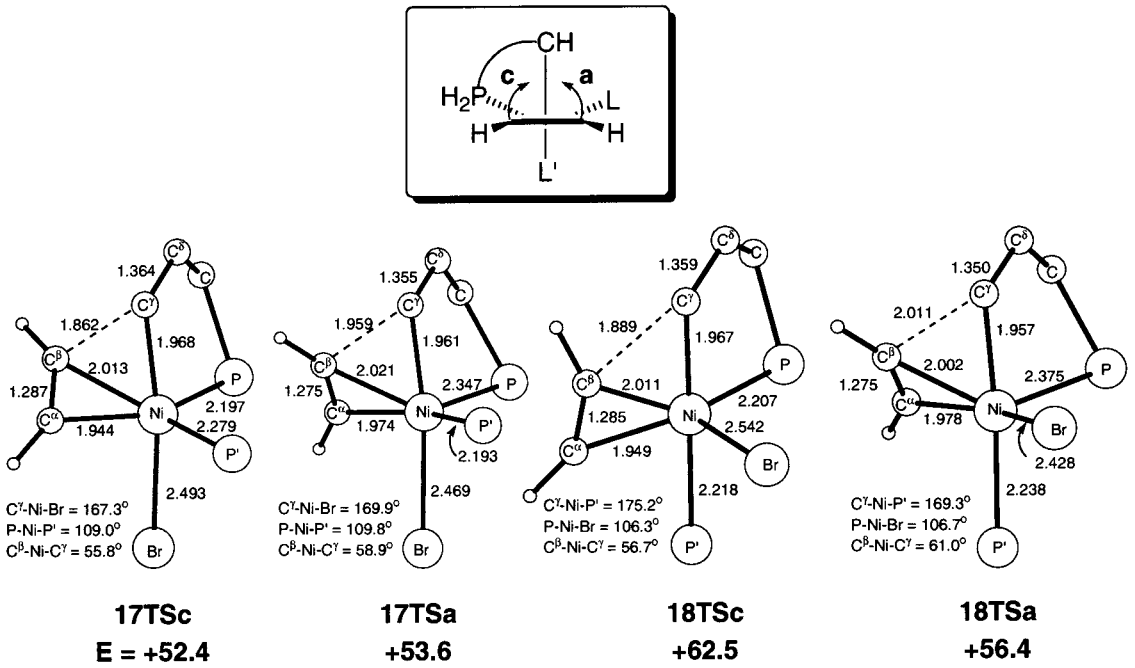

Figure 2. Optimized transition state geometries (distances in Å and angles in deg) and relative energies (kJ/mol) for acetylene insertion from **17** and **18** via clockwise (**c**) or anticlockwise (**a**) rotations. Phosphine and metallacycle hydrogen atoms have been omitted for clarity.

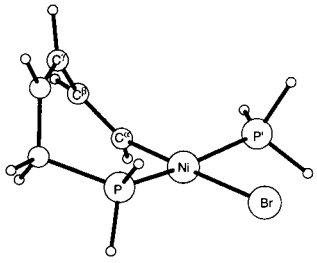

	Computed		
	R = H	R = CO_2H	Experimental
Ni - Br	2.410	2.410	2.3544 (3)
Ni - P'	2.187	2.193	2.2167 (5)
Ni - P	2.148	2.145	2.1799 (5)
Ni - C^{α}	1.883	1.893	1.9049 (18)
C^{α} - C^{β}	1.353	1.360	1.337 (3)
P' - Ni - P	168.3°	168.9°	167.979 (19)°
C^{α} - Ni - Br	177.8°	177.8°	175.15 (6)°
Br - Ni - P	87.0°	86.6°	91.017 (14)°
Br - Ni - P'	86.8°	86.7°	87.680 (14)°

Figure 3. Comparison of optimized geometries (distances in Å and angles in deg) for [NiBr{C(R)=CHCH=$CHCH_2PH_2$-$\kappa C,P$}(PH_3)] (R = H (**19**), CO_2H (**19c**)) with the experimental structure of [NiBr{*o*-C(CO_2Me)=$CHC_6H_4CH_2PPh_2$-$\kappa C,P$}-($PPhBz_2$)] (**5b**) (taken from ref 14).

incomplete modeling of the bulky phosphine groups in our present calculations. The data for the optimized structure of the analogue [NiBr{C(CO_2H)=CHCH=$CHCH_2PPh_2$-$\kappa C,P$}(PH_3)] (**19c**) (see below) are also given in Figure 3 for comparison, but the inclusion in the calculations of the CO_2H group at the α-position resulted in only minor structural changes. The computed energy of **19** (−170.9 kJ/mol) shows the overall acetylene insertion process to be strongly exothermic.

Geometries and energies for stationary points specific to the 4-coordinate mechanism (pathway **B** in Scheme 2) are shown in Figure 4. Phosphine displacement costs 29.5 kJ/mol and produces [NiBr(CH=$CHCH_2PH_2$-$\kappa C,P$)(η^2-C_2H_2)] (**20**), in which the Ni exhibits a distorted-square-planar geometry and the alkyne ligand is partially rotated out of the coordination plane (torsion angle $C^{\beta}-C^{\alpha}-Ni-C^{\gamma} = 54.4°$). At the insertion transition state (**20TS**), this torsion angle is reduced to 40.0°, similar to the value found for the associative mechanism **A**, reiterating the fact that the alkyne prefers attack from above the metallacyclic ring rather than a coplanar arrangement. Geometric changes equivalent to those described above for the 5-coordinate transition states are computed, but the energy of the 4-coordinate transition state is 18.2 kJ/mol higher than the lowest transition state located along the associative pathway (**17TSa**). The insertion produces initially a 3-coordinate intermediate showing a Y-shaped coordination geometry at Ni, **21**, in which the seven-membered metallacycle again displays a boat conformation. This arrangement promotes π-stabilization of the unsaturated species, as expected for a d^8 ML_3 species,[29] which is supported by the short computed Ni−Br distance (2.266 Å). Despite this, insertion to give the 3-coordinate product is much less favored than direct insertion via an associative mechanism and the re-addition of PH_3 to give the product **19** is very exothermic.

In summary, the overall insertion reaction of acetylene with [NiBr(CH=$CHCH_2PH_2$-$\kappa C,P$)(PH_3)] (**16**) is strongly favored thermodynamically. An associative 5-coordinate mechanism is kinetically preferred over a

(29) Albright, T. A.; Burdett, J. K.; Whangbo, M.-H. *Orbital Interactions in Chemistry*; Wiley: New York, 1985.

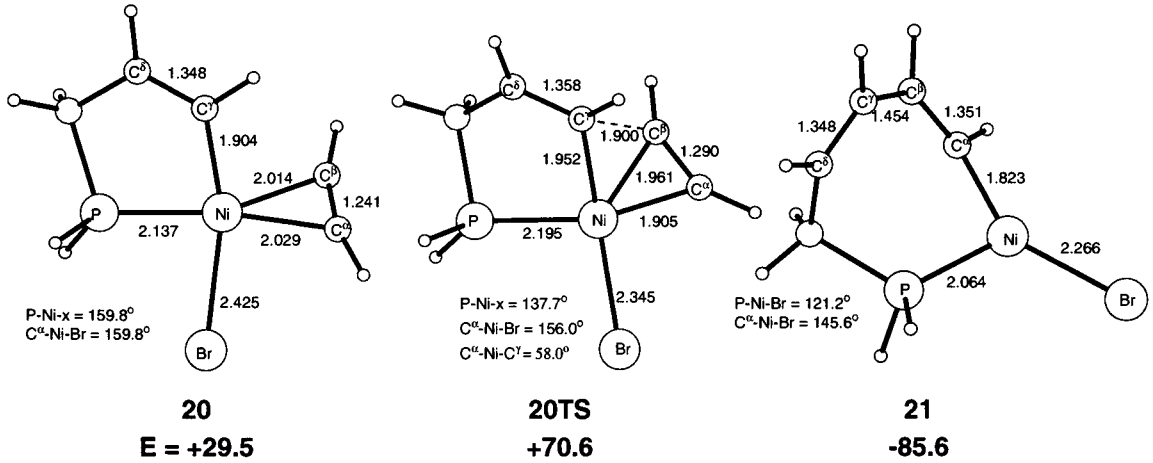

Figure 4. Optimized geometries (distances in Å and angles in deg) and relative energies (kJ/mol) for stationary points computed for the acetylene insertion reaction with [NiBr(CH═CHCH$_2$PH$_2$-$\kappa C,P$)(PH$_3$)] (**16**) via a 4-coordinate mechanism.

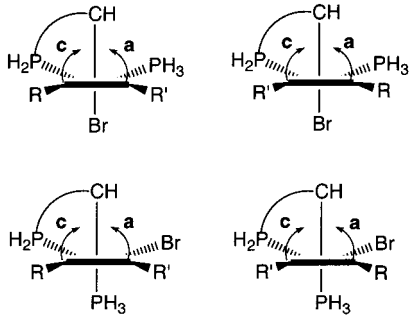

Figure 5. Structures of possible 5-coordinate intermediates and alkyne insertion pathways for the reaction of unsymmetrical alkynes, RC≡CR′, with [NiBr(CH═CHCH$_2$-PH$_2$-$\kappa C,P$)(PH$_3$)] (**16**) (**c** = clockwise rotation of the alkyne, **a** = anticlockwise).

4-coordinate mechanism involving initial phosphine displacement. This finding is consistent with the results of a kinetic study on the insertion reactions of alkynes with the related [NiCl(2-C$_6$H$_4$CH$_2$PR$_2$-$\kappa C,P$)(PR$_3$)] complexes.[10a] In addition, two relevant 5-coordinate intermediates have been located and the four related transition state structures derived from the latter have been found to be close in energy. In terms of modeling the regioselectivity of insertion with unsymmetrical alkynes, this preliminary study indicates that the location of all transition states, derived from analogues of both intermediates **17** and **18**, will be required and the results are discussed below.

(b) Fully Optimized Insertion Reactions of HC≡CMe, HC≡CCO$_2$H, and MeC≡CCO$_2$H with 16. The associative reaction of unsymmetrical alkynes with **16** produces initially two pairs of 5-coordinate intermediates analogous to **17** and **18** (Br or PH$_3$ axial, respectively), which differ in the position of the alkyne substituents. As a consequence, a total of eight insertion pathways must be considered as each 5-coordinate species generates two transition state structures (Figure 5). Relative energies for the 5-coordinate intermediates formed between **16** and HC≡CMe, HC≡CCO$_2$H, and MeC≡CCO$_2$H and for the resulting, fully optimized transition states are given in Figure 6, together with the results obtained for HC≡CH for comparison. With HC≡CMe, alkyne binding is slightly weaker and transition state energies are generally higher than those of HC≡CH. In contrast, the presence of a CO$_2$H substituent leads to significantly stronger alkyne binding energies and generally lower transition state energies, especially when Br is axial, and this result is consistent with qualitative observations of greater reactivity of ester-activated alkynes vs alkyl- and aryl-substituted ones when added to **1a**,**b**. The range of transition state energies exhibited in Figure 6 (approximately 35−70 kJ/mol) is consistent with the experimentally determined activation enthalpies for the reaction of PhC≡CCO$_2$Et with [NiCl(2-C$_6$H$_4$CH$_2$PR$_2$-$\kappa C,P$)(PR$_3$)] complexes.[10a] Trends in insertion regioselectivities will be discussed below.

The assumption that a 5-coordinate mechanism is still preferred with substituted alkynes was also tested via computation of the alternative 4-coordinate pathways with HC≡CMe and HC≡CCO$_2$H. The results (Figure 7) again show that phosphine substitution is less favorable than the formation of 5-coordinate adducts. With HC≡CMe, the 4-coordinate transition state energies (**20bTS** vs **20b′TS**) indicate a preference (by 15.4 kJ/mol) for the formation of an α-substituted product, but the transition state leading to a β-substituted product (**20c′TS**) is preferred with HC≡CCO$_2$H (by 5.1 kJ/mol). However, all 4-coordinate transition states are significantly less stable than the corresponding lowest energy 5-coordinate ones (Figure 6); hence, only the 5-coordinate mechanism will be studied with the remaining alkynes.

In comparison to the 4-coordinate reaction of HC≡CH, the overall insertion process is more favorable with HC≡CCO$_2$H but slightly less so with HC≡CMe. The different insertion regioselectivities have little effect on the energy of the respective insertion products (**19b,c** vs **19b′,c′**). However, with HC≡CCO$_2$H, a stabilization of the initial 3-coordinate product **21c** having CO$_2$H in the α-position was computed. Here a T-shape geometry is found at Ni and the structure shows evidence for stabilization via interaction of the metal center with the carboxylic acid ketonic oxygen (Ni···O = 2.083 Å).

(c) Regioselectivities for the Insertion Reactions of Unsymmetrical Alkynes, RC≡CR′ (R = H, R′ = Me, CF$_3$, Ph; R = Me, R′ = Ph; R = CO$_2$H, R′ = H, Me, CF$_3$, Ph), with 16. The studies described above support an associative mechanism for alkyne insertion

5-coordinate Intermediates

R = R' = H	-4.6			+14.5			
R = H, R' = Me	-1.5	+0.6		+19.0	+16.2		
R = CO_2H, R' = H	-16.1	-16.9		+6.1	+2.0		
R = CO_2H, R = Me	-12.2	-9.5		+16.9	+4.9		

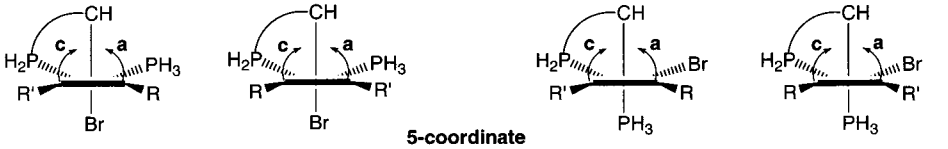

5-coordinate Transition States

	R' to β (a)	R' to α (c)	R' to α (c)	R' to β (a)	R' to β (c)	R' to α (a)	R' to α (c)	R' to β (a)
R = R' = H	+52.4	+53.6	–	–	+62.5	+56.4	–	–
R = H, R' = Me	+67.2	+58.2	+51.2	+67.5	+77.1	+67.4	+65.6	+68.1
R = CO_2H, R' = H	+44.6	+46.0	+39.1	+49.7	+39.7	+56.3	+50.1	+37.6
R = CO_2H, R' = Me	+64.8	+52.7	+41.8	+66.6	+61.1	+68.9	+57.2	+51.7

Figure 6. Relative energies (kJ/mol) for 5-coordinate intermediates and fully optimized transition states computed for the reactions of [NiBr(CH═CHCH$_2$PH$_2$-$\kappa C,P$)(PH$_3$)] (**16**) with HC≡CMe, HC≡CCO$_2$H, and MeC≡CCO$_2$H (**c** = clockwise rotation of the alkyne, **a** = anticlockwise). For each set of results the summed energies of **16** and the appropriate alkyne are set to zero.

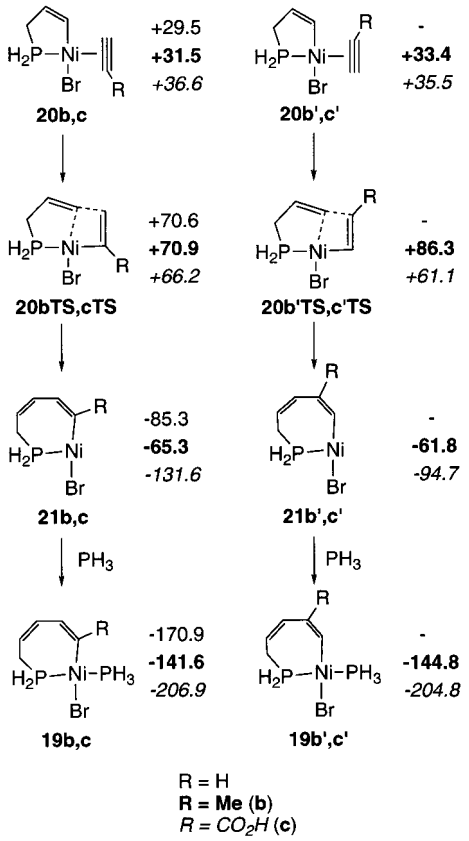

Figure 7. Relative energies (kJ/mol) for stationary points computed for the insertion reactions of [NiBr(CH═CHCH$_2$-PH$_2$-$\kappa C,P$)(PH$_3$)] (**16**) with HC≡CH (plain text), HC≡CMe (boldface text), and HC≡CCO$_2$H (italic text) via a 4-coordinate mechanism.

with **16** and suggest that the regioselectivity of the reaction is determined by kinetic factors. Therefore, in this part only 5-coordinate transition state structures and energies, calculated using the constrained-geometry approach described in section 2, will be considered.

(i) Alkyl- and Aryl-Substituted Alkynes. The transition state energies computed with these alkynes are given in Table 1, where, for each set of results, energies are given relative to the most stable of the eight transition states. For HC≡CMe (entry 1), the most accessible transition state is derived from the isomer having Br axial, in which the alkyne methyl group is adjacent to the PH$_3$ ligand and the alkyne undergoes a clockwise (**c**) rotation. This would lead ultimately to a product bearing the methyl substituent in the α-position, consistent with experimental observations on the reaction of HC≡C^{t}Bu with [NiBr(*o*-C$_6$H$_4$CH$_2$PPh$_2$-$\kappa C,P$)-(PR$_3$)] species (e.g. **10a** in Scheme 1). A second insertion transition state favoring a similar α-regioselectivity and which is close in energy (E = +7.2 kJ/mol) is also computed from the alternative isomer (Me adjacent to PH$_2$, **a** rotation). The two transition states with Br axial, leading to a β-substituted product, are around +16 kJ/mol higher in energy. For the transition states derived from the 5-coordinate precursor having PH$_3$ axial, an α-regioselectivity is again predicted for both possible alkyne orientations. However, all four transition states with PH$_3$ axial are at least 14 kJ/mol above the most stable pathway.

With HC≡CCF$_3$ (entry 2), the most stable transition state is derived from the axial PH$_3$ isomer having CF$_3$ adjacent to PH$_2$ and results from an anticlockwise (**a**) rotation of the alkyne. This would lead to an α-regioselectivity in the product, which is in contrast with the reaction of this alkyne with **1b** in which this geometry corresponds to the minor product **14b**.[30] However, a transition state derived from the axial-Br isomer leading to the alternative β-substituted product is separated by less than 2 kJ/mol from the favored TS: hence, the product mixture observed experimentally. In addition, when comparing the insertion reactions of HC≡CMe and HC≡CCF$_3$ arising from the axial-Br intermediates, a change in regioselectivity is predicted.

Computed energies for the insertion of HC≡CPh (entry 3) from all four possible 5-coordinate intermediates favor transition states leading to an α-substituted product. The most stable is derived from an axial-Br isomer where the phenyl group is adjacent to PH$_3$ and the alkyne rotates clockwise (**c**). The calculations are therefore consistent with experimental results (cf. **11a**,**b**)

Table 1. Relative Transition State Energies (kJ/mol) for the Insertion Reactions of Unsymmetrical Alkyl- and Aryl-Substituted Alkynes, RC≡CR′, with [NiBr(CH=CHCH$_2$PH$_2$-κ*C,P*)(PH$_3$)] (16) via an Associative Mechanism (c = Clockwise Rotation of the Alkyne, a = Anticlockwise)[a]

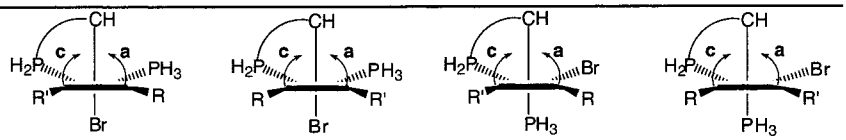

Entry		R′ to β (c)	R′ to α (a)	R′ to α (c)	R′ to β (a)	R′ to β (c)	R′ to α (a)	R′ to α (c)	R′ to β (a)
1	R = H, R′ = Me	+16.0	+7.2	**+0.0**	+16.2	+26.2	+16.1	+14.5	+16.7
2	R = H, R′ = CF_3	+1.9	+7.2	+2.9	+4.6	+11.9	**+0.0**	+7.6	+11.6
3	R = H, R′ = Ph	+28.4	+11.1	**+0.0**	+29.5	+41.0	+17.5	+15.3	+28.9
4	R = Me, R′ = Ph	+11.7	+10.1	**+0.0**	+20.0	+29.0	+13.4	+16.6	+25.5
5	R = CO_2H, R′ = Ph	+32.7	+12.2	**+0.0**	+37.2	+16.3	+25.2	+12.2	+17.3

[a] For each alkyne the most stable transition state structure is assigned an energy of 0.0 kJ/mol.

Table 2. Relative Transition State Energies (kJ/mol) for the Insertion Reactions of Unsymmetrical Alkynes, RC≡CR′ (R = CO_2H, R′ = H, Me, CF_3, Ph), with [NiBr(CH=CHCH$_2$PH$_2$-κ*C,P*)(PH$_3$)] (16) via an Associative Mechanism (c = Clockwise Rotation of the Alkyne, a = Anticlockwise)[a]

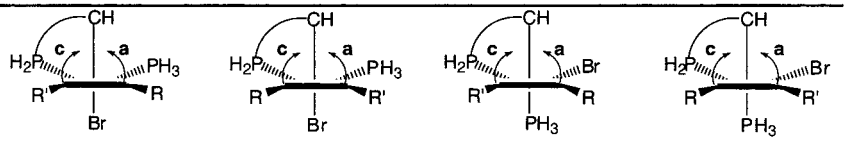

Entry		R′ to β (c)	R′ to α (a)	R′ to α (c)	R′ to β (a)	R′ to β (c)	R′ to α (a)	R′ to α (c)	R′ to β (a)
1	R = CO_2H, R′ = H	+7.8	+8.1	+2.7	+13.0	+1.7	+19.0	+13.7	**+0.0**
2	R = CO_2H, R′ = Me	+21.9	+10.7	**+0.0**	+25.3	+19.2	+27.8	+16.2	+9.9
3	R = CO_2H, R′ = CF_3	+7.6	+10.5	+3.8	+15.0	**+0.0**	+13.2	+12.9	+3.6
4	R = CO_2H, R′ = Ph	+32.7	+12.2	**+0.0**	+37.2	+16.3	+25.2	+12.2	+17.3

[a] For each alkyne the most stable transition state structure is assigned an energy of 0.0 kJ/mol.

obtained for the reactions of HC≡CPh with [NiBr(*o*-C$_6$H$_4$CH$_2$PPh$_2$-κ*C,P*)(PR$_3$)] species. For both MeC≡CPh and HO_2CC≡CPh (entries 4 and 5), the lowest energy transition state is equivalent to that found with HC≡CPh, again predicting the phenyl group to occupy the α-position in the products. However, for MeC≡CPh, one transition state giving an alternative regioselectivity is found at +11.7 kJ/mol. For HO_2CC≡CPh the transition states leading to the *β*-phenyl isomer are high in energy (>16 kJ/mol), but the differences in energy between alternative regiopathways are dramatically reduced with the axial-PH_3 isomers. Experimentally, the reaction of EtC≡CPh with [NiBr(*o*-C$_6$H$_4$CH$_2$PPh$_2$-κ*C,P*)(PR$_3$)] species is not completely regiospecific (**12b**/**13b**), consistent with the possible accessibility computed for alternative insertion transition states. In agreement with the calculations, RO_2CC≡CPh alkynes give only products with phenyl in the α-position.

(ii) Insertion Reactions with HO_2CC≡CR′ (R′ = H, Me, CF_3, Ph). Computed relative energies for transition states formed between these alkynes and **16** are given in Table 2. For HO_2CC≡CH, the most accessible transition state is derived from an axial-PH_3 isomer in which the carboxylic acid group is adjacent to PH_2 and the alkyne rotates anticlockwise, leading ultimately to an α-substituted product. For the alternative isomer with PH_3 axial, the same insertion regioselectivity is clearly favored. However, when insertion occurs from the species with Br axial, formation of the other regioisomer is preferred, with the lowest energy transition state being only +2.7 kJ/mol higher than that of the preferred route. Experimentally, the insertion reactions of RO_2CC≡CH alkynes with [NiBr(*o*-C$_6$H$_4$CH$_2$-PPh$_2$-κ*C,P*)(PR$_3$)] species are sensitive to the nature of

(30) Unpublished results. The reaction mixture obtained from diffusion of HC≡CCF$_3$ into a solution of **1b** was very unstable (see also ref 14) but could be shown spectroscopically to contain the two α- and *β*-insertion products **14b** and **15b** in the ratio 1:2.5 (yield >90%). The regioisomers could be deducted from the magnitude of the PP couplings measured by ^{31}P NMR spectroscopy, as it was known from ref 14 that the presence of an electron-withdrawing group in the *β*-position leads to a smaller value of this coupling. Attempted crystallization led to complete decomposition of **14b**, most likely due to *β*-hydride elimination, but single crystals obtained for **15b** confirmed the location of the CF_3 on the *β*-carbon (Edwards, A. J.; Wenger, E. *Acta Crystallogr., Sect. C*, submitted for publication). **14b**: ^{19}F NMR (188.2 MHz, C_6D_6) δ −53.8 (s, CF_3); ^{31}P{^{1}H} NMR (81.0 MHz, CD_2Cl_2) δ 9.1 (br d, $^2J_{PP}$ = 335.0 Hz, PPhBz$_2$), 31.6 (dq, $^2J_{PP}$ = 335.0, $^5J_{PF}$ = 3.1 Hz, PPh$_2$). **15b**: ^{1}H NMR (300 MHz, CD_2Cl_2) δ 3.06−3.30 (m, 4H, CH_2P), 3.54 (dd, 1H, *J* = 12.3, 8.7 Hz, CH_2P), 3.70 (dd, 1H, *J* = 14.4, 7.2 Hz, CH_2P), 6.70 (br d, 1H, *J* = 6.6 Hz), 6.99 (d, 2H, *J* = 6.9 Hz), 7.10−7.68 (m, 25H), 8.11 (ddd, 2H, *J* = 9.6, 7.8, 1.5 Hz); ^{19}F NMR (188.2 MHz, C_6D_6) δ −63.7 (app t, $^4J_{PF}$ = 5.8 Hz, CF_3); ^{31}P{^{1}H} NMR (81.0 MHz, CD_2Cl_2) δ 10.1 (dq, $^2J_{PP}$ = 305.2, $^4J_{PF}$ = 5.3 Hz, PPhBz$_2$), 36.5 (dq, $^2J_{PP}$ = 305.2, $^4J_{PF}$ = 5.7 Hz, PPh$_2$).

Table 3. Carbon p-Orbital Contributions (%) to the π HOMO ($\pi_\perp$) and Second HOMO ($\pi_{||}$) of Alkynes RC≡C′R′ (with Resulting Regioselectivities Given in Parentheses) and Energy Differences (ΔE(TS), kJ/mol) between the Lowest Energy Alternative Insertion Transition States (Preferred Regioselectivities from the Transition State Calculations Given in Parentheses)[a]

			% contribn					
entry	RC≡C′R′		C	C′	($\pi_\perp$ regio)	ΔE(TS)	(TS regio)	exptl regio
1	R = H, R′ = CH_3		48.0	40.3	(R′ to α)	16.2	(R′ to α)	R′ to α[c]
2	R = H, R′ = CF_3		44.7	46.2	(R′ to β)	1.9	(R′ to α)	R′ to β
3	R = H, R′ = Ph	$\pi_\perp$	29.1	12.6	(R′ to α)	28.4	(R′ to α)	R′ to α
		$\pi_{||}$	47.1	44.2				
4	R = Me, R′ = Ph	$\pi_\perp$	27.5	16.5	(R′ to α)	11.7	(R′ to α)	R′ to α
		$\pi_{||}$	39.2	44.0				
5	R = CO_2H, R′ = Ph	$\pi_\perp$	25.9	8.5	(R′ to α)	16.3	(R′ to α)	R′ to α[d]
		$\pi_{||}$[b]	37.9	28.7				
6	R = CO_2H, R′ = H	$\pi_\perp$	38.2	38.6	(R′ to β)	2.7	(R′ to β)	R′ to β[d]
		$\pi_{||}$[b]	41.2	34.2				
7	R = CO_2H, R′ = Me	$\pi_\perp$	41.1	32.9	(R′ to α)	9.9	(R′ to α)	R′ to α[d]
		$\pi_{||}$[b]	34.0	21.8				
8	R = CO_2H, R′ = CF_3	$\pi_\perp$	29.5	32.5	(R′ to β)	3.8	(R′ to β)	R′ to β[d]
		$\pi_{||}$[b]	40.3	34.9				

[a] Preferred experimental regioisomers (exptl regio) for related alkynes are also given for comparison. [b] When R = CO_2H, the $\pi_{||}$ orbital is the third HOMO of the system, the second HOMO being located primarily on the CO_2H group. [c] Regioselectivity for HC≡C^{t}Bu, as no experimental results for HC≡CMe are available. [d] R = CO_2Me, CO_2Et, $CO_2{}^t$Bu (see Scheme 1).

both the substituents on the alkyne and the auxiliary phosphine with changes from an α- to a β-regioselectivity being observed with increased steric demands. The energetic proximity of two alternative regiopathways therefore appears consistent with these observations. It is also interesting to note that this alkyne is computed to behave similarly to HC≡CCF_3. Both favor α-substituted products arising from an axial-PH_3 precursor via anticlockwise alkyne rotation. An axial-PH_3 precursor is also computed to be preferred for HO_2CC≡CCF_3, although in this case a clockwise rotation is favored (see below).

With HO_2CC≡CMe the lowest energy transition state is derived from an axial-Br isomer with the Me group adjacent to PH_3 and arises via clockwise rotation of the alkyne to give a product with Me in the α-position. A similar preference is computed from the other isomer with Br axial, but a change in regioselectivity is predicted if insertion occurs from 5-coordinate intermediates with PH_3 axial. The most accessible of these transition states is at +9.9 kJ/mol, and the relative accessibility of this alternative pathway is again consistent with the sensitivity toward steric effects of the reactions of MeO_2CC≡CMe with either **1a** or **1b**.

For HO_2CC≡CCF_3 three low-energy transition states are computed. Two (E = 0.0 and +3.6 kJ/mol) are derived from the axial-PH_3 intermediates. They lead to the product having CF_3 in the β-position, which would be in agreement with the only regioisomer (**9b**) obtained experimentally from reaction with **1b**. However, a third transition state quite close in energy (E = +3.8 kJ/mol), resulting from an axial-Br species, favors the opposite regioisomer and in this case a mixture of regioisomers would be expected.[31]

Thus far, for three of the four HO_2CC≡CR′ alkynes a change in regioselectivity occurs when the Br and PH_3 ligands swap positions. The exception is HO_2CC≡CPh, but even here a dramatic reduction in the energy between alternative regiopathways occurs with the axial-PH_3 isomers. One reason that a swap in regioselectivity may not occur with HO_2CC≡CPh is that it has highly polarized π-orbitals (see below).

(31) Some computations were carried out with use of PMe_3 in optimization instead of PH_3 in order to assess whether a more realistic phosphine would increase the energy gap between the transition states, but no significant difference was observed.

3. Discussion

(i) Computed and Experimental Regioselectivities. The results obtained from DFT calculations have shown that the different transition state energies for the associative alkyne insertion process seem to determine the regioselectivities of the reaction and the computed results reproduce successfully the experimental trends. Generally, the lowest energy transition state is consistent with the preferred or only regioisomer observed experimentally with analogous alkynes, the only exception being HC≡CCF_3. The experimental ratio between the different isomers can be correlated to the energy differences between the two lowest energy transition states leading to opposite regioisomers (ΔE(TS), Table 3). Energy differences smaller than 3 kJ/mol are computed for HC≡CCF_3 and HO_2CC≡CH (entries 2 and 6), and these results are consistent with the mixture of isomers obtained experimentally and with the sensitivity of the insertion of RO_2CC≡CH to steric effects. It may be that the small preference toward a α-substituted product computed for the insertion of HC≡CCF_3 could be overturned by such steric factors, hence explaining the experimental results observed with **1b**. With larger energy differences (ΔE > 16 kJ/mol), the corresponding experimental insertions are generally regiospecific. The only other discrepancy in the computed data is the very small energy difference obtained for CF_3C≡CCO_2H (3.8 kJ/mol), which is clearly inconsistent with the regiospecificity seen experimentally between CF_3C≡CCO_2Et and [NiBr(*o*-$C_6H_4CH_2PPh_2$-κ*C*,*P*)(PPhBz$_2$)] (**1b**), the only product being that with CF_3 in the β-position (**9b**).[31]

(ii) Orbital Analysis of the Alkyne Insertion Process. As with theoretical studies of alkyne insertion reactions in general, few orbital analyses of this process have been published. Most discussion has been based upon work on alkene insertion reactions, especially as computed alkyne insertion transition states have tended

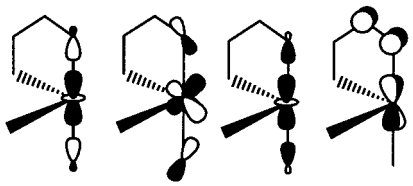

Figure 8. Schematic representations of the LUMO (**24**) and bonding Ni−C$^{\alpha}$ orbitals (**25**−**27**) computed for the fragment {NiBr(CH═CHCH$_2$PH$_2$-$\kappa C,P$)(PH$_3$)}.

to exhibit planar four-centered geometries similar to those located with alkenes. Thorn and Hoffmann's early EHMO analysis of alkene insertion into Pt−H bonds focused on the role of the alkene π* orbital within two C···H antibonding interactions that develop during the insertion process.[27] As shown in eq 1, the C···H anti-

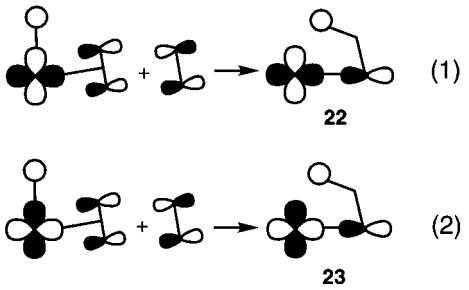

bonding contribution is alleviated in **22** by an admixture of the alkene π* orbital, hence reducing the destabilization of this orbital which eventually evolves into the M−C$^{\alpha}$ σ-bonding orbital. In **23** (eq 2), the C···H antibonding interaction is again reduced by the alkene π* orbital but this time at the expense of an increased M−C$^{\alpha}$ σ-antibonding character. For alkene insertion to be facile, orbitals analogous to **23** must be vacant. Subsequent workers[16,32] have stressed charge-transfer interactions between the M−R σ-bond involved in the insertion reaction and the alkene/alkyne π* orbitals and between the M−R σ*-bond and the alkene/alkyne π orbitals. A similar picture was used by Nakatsuji and co-workers in their proposed dual frontier orbital control of alkyne insertion and regioselectivity in the Pd-catalyzed silastannation of alkynes (see Introduction).[17]

To compare these models with the reactions discussed in this paper and in an attempt to understand the origins of the computed and experimental regioselectivities, we have performed an electronic structural analysis of the insertion reactions of HC≡CH via the 5-coordinate intermediates **17** and **18** to assess the extent of frontier orbital control in these systems. In our approach the total molecule is built up from the fragments {NiBr(CH═CHCH$_2$PH$_2$-$\kappa C,P$)(PH$_3$)} and {HC≡CH}, which allows us to probe how these two components interact. We have focused on the insertions arising from clockwise rotation of the alkyne and have monitored the evolution of the molecular orbitals as a function of the C$^{\beta}$−Ni−C$^{\gamma}$ angle. For **17**, an analysis of the orbitals of the initial {NiBr(CH═CHCH$_2$PH$_2$-$\kappa C,P$)-(PH$_3$)} fragment shows the LUMO of the system (**24**) to contain significant Ni−C$^{\gamma}$ σ-antibonding character (Figure 8). Ni−C$^{\gamma}$ bonding character is distributed between three fragment orbitals: Two of these (**25**, **26**) are Br−Ni−C$^{\gamma}$ σ-bonding, but the third (**27**) is dominated by Ni−C$^{\gamma}$ π-bonding character. In the case of the alkyne, due to the nonplanar transition state configuration, both the $\pi_{\|}$ and $\pi_{\perp}$ orbitals overlap with these metal fragment orbitals. Only one of the alkyne LUMOs interacts significantly ($\pi_{\|}$*), as the $\pi_{\perp}$* orbital lies to much higher energy.

Although the low symmetry of the system and the number of orbitals involved make analysis difficult, some key features in the electronic structure of **17TSc** can be highlighted. In particular, the participation of the unoccupied orbitals of both fragments is rather limited. Significant mixing of the Ni−C$^{\gamma}$ σ* orbital (**24**) and the alkyne π orbitals occurs only in the HOMO of the transition state; however, the overall interaction between C$^{\beta}$ and C$^{\gamma}$ in this orbital is antibonding (MO 33, Figure 9). This is contrary to the model proposed for alkyne insertion into Pd−Sn bonds by Nakatsuji et al., where a bonding interaction was identified,[33] but is more closely related to interaction **23** highlighted by Thorn and Hoffmann, although no alkyne π* character is evident in the present case. Mixing of the alkyne $\pi_{\|}$* LUMO with the Ni−C$^{\gamma}$ bonding orbitals (**25**−**27**) also only occurs to any significant extent in one occupied orbital (MO 27). This orbital also features alkyne π character and is equivalent to interaction **22** identified by Thorn and Hoffmann as being responsible for the formation of the new Ni−C$^{\alpha}$ σ-bond (note that as the contour plot of MO 27 is drawn in the C$^{\beta}$−Ni−C$^{\gamma}$ plane the antibonding C$^{\beta}$···C$^{\gamma}$ interaction is highlighted rather than the Ni−C$^{\alpha}$ bonding component). MO 27 can be considered equivalent to the Pd−alkyne back-bonding interaction highlighted by Nakatsuji et al., which is responsible for overall alkyne reactivity. In addition, MO 27 also exhibits a significant amount of Ni−PH$_2$ σ-bonding character. In both MOs 33 and 27 the alkyne contribution is dominated by the $\pi_{\perp}$ orbital.

To much lower energy, a number of orbitals (most importantly MOs 22 and 16) exhibit significant C$^{\beta}$···C$^{\gamma}$ bonding character. These orbitals arise from bonding overlap between occupied alkyne π and both the Ni−C$^{\gamma}$ σ- and π-bonding orbitals. In MO 22, roughly equal amounts of $\pi_{\perp}$ and $\pi_{\|}$ character are present, but in MO 16 the alkyne contribution is mostly derived from $\pi_{\|}$. The ability of the Ni−C$^{\gamma}$ π-bond **(27)** to become involved in C$^{\beta}$−C$^{\gamma}$ bond formation is consistent with the nonplanar transition states computed for insertion into a Ni−vinyl bond.

Orbitals related to those highlighted above for **17TSc** can also be seen in the electronic structure of **18TSc**. One possibly significant difference is seen in MO 28 (equivalent to MO 27 of **17TSc**) where mixing in of Ni−Br σ-bonding character is computed, instead of Ni−PH$_2$ bonding character. This observation may be related to the change in regioselectivities often computed when the Br and PH$_3$ ligands swap positions.

To summarize, the results above indicate that the $\pi_{\perp}$ orbital of the alkyne plays an important role in the insertion process; hence, its electronic distribution will

(32) Koga, N.; Obara, S.; Kitaura, K.; Morokuma, K. *J. Am. Chem. Soc.* **1985**, *107*, 7109.

(33) In ref 17 analysis was not performed on the transition state stucture but rather a model in which the metal−alkyne distance was lengthened to 3 Å. This could possibly account for the different nature of the orbitals computed in the present study.

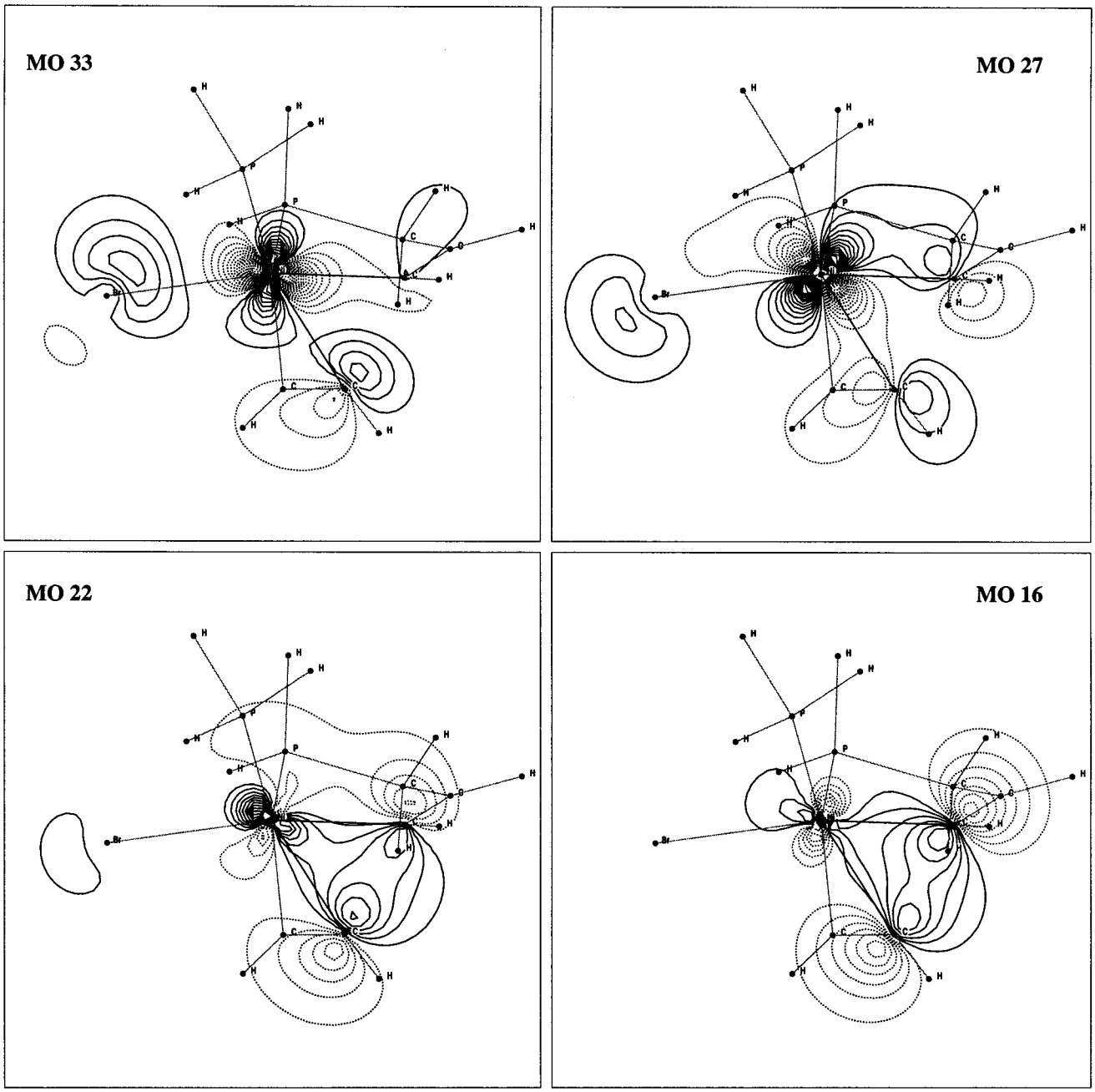

Figure 9. Electron density contour plots for key orbitals involved in $C^{\beta}-C^{\gamma}$ interactions. Orbitals are plotted in the plane containing the $C^{\beta}-Ni-C^{\gamma}$ moiety.

affect the regiochemistry of the reaction. However, significant interactions between the metal and alkyne fragments are not limited to the frontier orbital region, suggesting that the model published by Nakatsuji for insertion into Pd−Sn bonds may be too simple for the present case.

(iii) Alkyne Orbital Polarizations and Regioselectivities. As already highlighted in the Introduction, an excellent correlation exists between the electronic distribution of the $\pi_{\perp}$ orbitals of alkynes and the regioselectivity of their insertions, as observed experimentally during their reactions with **1a,b**. Included in Table 3 are the computed distributions of both the $\pi_{\perp}$ and $\pi_{||}$ orbitals of the free alkynes, to be compared with the computed transition state energy differences between alternative regiopathways. The data support our earlier conclusion, which was that the lower energy insertion pathway generally is the one in which the new C−C bond formed involves the alkyne carbon atom bearing the larger $\pi_{\perp}$ p-orbital contribution. A borderline case is illustrated by HC≡CCF$_3$ (entry 2), where the $\pi_{\perp}$ polarization model predicts a product having CF$_3$ in the β-position, in agreement with experiment, whereas the results from the computed transition states favor the α-product. For some alkynes (e.g. HC≡CMe, HC≡CPh, and HO$_2$CC≡CPh, entries 1, 3, and 5, respectively), large $\pi_{\perp}$ polarizations lead to relatively large energy differences between regiopathways. However, the correlation is not precise, as similarly large $\pi_{\perp}$ polarizations are computed for MeC≡CPh and HO$_2$CC≡CMe, whereas smaller energy differences are produced. In general, the polarization of the $\pi_{||}$ orbitals is in the same

direction as that computed for $\pi_\perp$, although there are some exceptions (MeC≡CPh, $HO_2CC{\equiv}CH$, and $HO_2CC{\equiv}CCF_3$).

When we analyze more closely the alkyne $\pi_\perp$ polarization model in the light of the different intermediates and transition states described above, it appears that poorly polarized alkynes seem to favor transition states having the PH_3 group trans to the Ni−C bond; hence, the success of the model depends on the nature of the alkyne and the locations of the PH_3 and Br ligands in the 5-coordinate intermediate involved. For example, should the insertion arise from the intermediate in which Br is axial, the polarization and the TS models are in agreement for all five aryl- and alkyl-substituted alkynes (columns 1−4, Table 1), including $HC{\equiv}CCF_3$. When the corresponding insertions from the axial-PH_3 intermediates are considered (columns 5−8), the polarization model agrees with the computed regioselectivities for all but this last alkyne.

For the four alkynes bearing carboxylic acid substituents (Table 2), the role of the ligand trans to Ni−C becomes more important, as only $HO_2CC{\equiv}CPh$ preserves the same regioselectivity if Br and PH_3 are inverted, which may again be correlated to a strong $\pi_\perp$ orbital polarization. The alkyne $\pi_\perp$ polarization model correctly predicts β-CO_2H-substituted products for both $HO_2CC{\equiv}CPh$ and $HO_2CC{\equiv}CMe$, which are also the favored TS arising from axial-Br isomers. For both $HO_2CC{\equiv}CH$ and $HO_2CC{\equiv}CCF_3$, however, the regioselectivities obtained with the polarization model and from the lowest transition states, leading to products with the CO_2H group in the β-position, arise from axial-PH_3 isomers. It is interesting to note that for these two alkynes only a small polarization of the $\pi_\perp$ orbital was computed while the polarization of the $\pi_\parallel$ orbital is reversed.

Overall, for six of the eight alkynes studied, the $\pi_\perp$ polarization model predicts the same regioselectivities as those computed for insertions taking place from 5-coordinate axial-Br intermediates, the exceptions being $HO_2CC{\equiv}CH$ and $HO_2CC{\equiv}CCF_3$, which favor insertions from PH_3-axial intermediates, although the polarization model remains accurate. More generally, whenever electron-withdrawing groups are present, the regioselectivity of insertion appears sensitive to the nature of the ligand trans to the metal−vinyl bond and may change according to whether Br or PH_3 is axial in the transition state. Hence, predictions of the insertion regioselectivities for poorly polarized alkynes of this type turn out to be very difficult, as they will be greatly dependent on the nature of the intermediate from which the energetically favored insertion occurs and, therefore, on the nature of the auxiliary ligands present. Furthermore, for these alkynes, energy differences between alternative regiopathways may become small enough to be overcome by steric effects.

4. Conclusions

We have employed density functional calculations to study the insertion reactions of alkynes with the model nickelacycle [NiBr(CH═$CHCH_2PH_2$-$\kappa C,P$)(PH_3)]. The calculations indicate that insertion via 5-coordinate transition states is kinetically preferred, in agreement with previous experimental studies. With one exception (the trifluoromethyl alkyne $HC{\equiv}CCF_3$), computed transition state energies for a range of unsymmetrical alkynes can accurately reproduce the regioselectivities observed experimentally with analogous systems. Although the origins of those regiocontrols are not easily understood, these results show clearly that electronic factors are very important in determining the regiochemical outcome of these insertion reactions. A possible interaction between the carbon atom bonded to nickel and the $\pi_\perp$ orbital of the alkyne during the new C−C bond formation has been postulated. This proposition is supported by the accuracy of a simple predictive model for insertion regioselectivity based upon the polarization of the alkyne $\pi_\perp$ orbital. This approach generally predicts the experimental regioselectivities correctly, and closer analysis shows it is most successful for strongly polarized alkynes, which seem to favor insertion from 5-coordinate intermediates having Br trans to the Ni−vinyl bond. With alkynes featuring electron-withdrawing groups (CF_3, CO_2H), a swap in regioselectivity is generally computed for insertion proceeding from the 5-coordinate isomers having PH_3 in the axial position. Regioselectivities therefore depend on both the alkyne substituents and the nature of the 5-coordinate intermediate leading to the favored insertion transition state. In the case of alkynes with small polarizations, generating only small energy differences between the different transition states, the nature of the latter and the direction of the alkyne rotation needed to reach the transition state for insertion may well be subject to steric effects, and this factor will be investigated in future work.

Supporting Information Available: Tables giving computed energies and Cartesian coordinates for the various compounds discussed in this paper. This material is available free of charge via the Internet at http://pubs.acs.org.

OM010795Y